Impact of Occupancy-Based Buildings-to-Grid Integration on Frequency Regulation in Smart Grids

Bing Dong¹, Ahmad F. Taha², Nikolaos Gatsis², Zhaoxuan Li¹, and Ankur Pipri²

Abstract—The bulk of the produced electricity powers buildings; 120 million homes and 5 million commercial buildings dominate the U.S. energy consumption. Creative design of Buildings-to-Grid (BtG) integration methods is an essential component of smart cities. Buildings' occupancy behavior is a crucial component of successful BtG integration, as buildings become more sophisticated and people spend more time in offices and cities-making occupancy behavior one of the leading factors in energy consumption and thus largely impacting power grid dynamics. In this paper, we study the impact of integrating occupancy-based building dynamics and constraints with power grid transients, while focusing on frequency regulation. First, dynamics of building clusters and building-integrated power networks are presented—both operating at different time-scales. Second, occupancy-based building constraints are discussed. Third, the time-scale discrepancies are investigated, and a model predictive control-based algorithm that formulates occupancybased BtG integration is given. Finally, case studies demonstrate the impact of the proposed framework on energy savings and significant frequency regulation.

I. Introduction and Paper Contribution

Smart cities consist of sustainable and resilient infrastructures, where buildings are a major constituent. Building energy consumption contributes to more than 70% of electricity usage—profoundly impacting power grid's operation. Futuristic cities equipped with optimized building designs have the auspicious potential to play a pivotal role in reducing global energy consumption while maintaining stable electricgrid operations. As buildings are physically connected to the electric power grid, it is natural to understand their coupling and develop a framework for Buildings-to-Grid (BtG) integration. To understand the role of BtG integration, the authors in [1] provide a list of relevant research questions for successful BtG integration.

Various studies address a breadth of computational and experimental aspects of BtG integration. An overview of demand response potential from smart buildings is presented in [2]. An experimental high-level architecture that enables smart buildings is proposed in [3] with a focus on heating, ventilating, and air conditioning (HVAC) systems and grid integration. A bi-level optimization framework for commercial buildings integrated with a distribution grid is proposed in [4]. Detailed dynamic models for buildings with multiple zones (upper level) and an operational model for

the distribution grid with voltage/current balance equations (lower level) are included; nonetheless, a transient model of the power grid, capturing frequency deviation, is missing.

The regulation service provision by smart buildings is investigated in [5]. Other BtG integration studies have shown that grid-aware building HVAC controls can provide frequency regulation or other ancillary services to the grid [6]–[10], largely without sacrificing the occupants' comfort. The load-shifting capability of buildings has also been explored [11]. Explicit account of the grid dynamics and power flows is on the other hand missing from the previously mentioned works.

Occupancy behavior in buildings is becoming an important topic of research. Building systems become more sophisticated and people spend more time in buildings, making occupancy behavior one of the leading influencers of energy consumption in buildings [12] with large impacts on grid dynamical operation. This is due to the following reasons. (a) Significant interactions between occupants and building systems: The occupants expectation of comfort or satisfaction in the built environment drives the occupant to perform various controls, such as adjusting the thermostat in spaces, opening windows for ventilation [13], turning on lights [14], pulling down the window blinds [15], [16], and consuming domestic hot water [17]. (b) Strong coupling between occupant behavior and building performance: Various occupancy behaviors have different impacts on built environment (e.g., indoor temperature, humidity level, lighting, CO2, etc.) and energy end use [18]. In addition, prior studies have demonstrated that significant energy savings could be achieved through behavior driven predictive building controls [19]–[21].

To model building dynamics, a typical thermal resistance and capacitance circuit model can be used to represent heat transfer and thermodynamical properties of the building envelope—widely used in building climate control studies [22]–[25]. Given these models for building dynamics, various control routines have been developed for building controls. Currently, many commercial buildings use PID controllers for HVAC systems [26]. However, model predictive control (MPC) has proved to be advantageous when applied to building dynamics [27]–[30] with the majority of works showing significant energy savings given forecast and parametric uncertainty.

Unfortunately, none of the recent studies produces an occupancy-based formulation or routine that buildings and power grids operators can simultaneously utilize to optimize their performance explicitly coupling power grid and building

¹Department of Mechanical Engineering, ²Department of Electrical and Computer Engineering, The University of Texas at San Antonio, San Antonio, Texas. Emails: {Bing.Dong, Ahmad.Taha, Nikolaos.Gatsis, Zhaoxuan.Li, Ankur.Pipri}@utsa.edu. This material is based upon work supported by the National Science Foundation under Grant No. CBET-1637249.

control actions and operational decisions. The objective of this paper is to generate occupancy-based, local control actions/signals for buildings and power generators such that the overall performance is optimized in terms of stability, energy savings, and other socio-economic metrics. Specifically, we focus on frequency regulation and energy savings as the main high-level objectives. An extended version of this work without the occupancy-based modeling and constraints is presented in our recent work [31].

The paper is organized as follows. In Sections II, III, and IV, we present the dynamics of building clusters, occupancy building model, and the buildings-integrated power network. Optimal power flow is also integrated in these models. In Section V, we propose our approach of occupancy-based BtG integration optimization problem. A customized algorithm is also discussed to seamlessly include the optimal power flow into the integrated framework. Case studies with realistic building parameters are given in Section VI.

II. BUILDING CLUSTERS DYNAMICS

In this paper, we use a typical thermal resistance and capacitance (RC) network model to represent heat transfer and thermodynamics of building envelope, which has been widely used and accepted in building control studies [22]–[25]. This model is sufficient for a high-level BtG integration study. A typical three resistant and two capacitance (3R-2C) model is shown in [24]. The building dynamics with temperature states $T_{\rm wall}$ and $T_{\rm zone}$ can be written as:

$$\begin{split} \dot{T}_{\mathrm{wall}} &= \frac{T_{\mathrm{amb}} - T_{\mathrm{wall}}}{CR_{2}} + \frac{T_{\mathrm{zone}} - T_{\mathrm{wall}}}{CR_{1}} + \frac{\dot{Q}_{\mathrm{sol}}}{C} \\ \dot{T}_{\mathrm{zone}} &= \frac{T_{\mathrm{wall}} - T_{\mathrm{zone}}}{C_{\mathrm{zone}}R_{1}} + \frac{T_{\mathrm{amb}} - T_{\mathrm{zone}}}{C_{\mathrm{zone}}R_{\mathrm{win}}} + \frac{\dot{Q}_{\mathrm{int}} + \dot{Q}_{\mathrm{HVAC}}}{C_{\mathrm{zone}}}, \end{split}$$

where $R_{\rm win}$, R_2 , and R_1 are physical parameters of building envelope; C is a lumped thermal capacity of all walls and roof; $C_{\rm zone}$ is the thermal capacity of the zone; $\dot{Q}_{\rm sol}$ is the total absorbed solar radiation on the external wall; $\dot{Q}_{\rm int}$ is the total internal heat gains from space heat sources such as desktop, people, and lights; $T_{\rm amb}$, $T_{\rm zone}$, and $T_{\rm wall}$ are the outside ambient, wall, and zone/space temperatures, respectively. The cooling load can be calculated as $\dot{Q}_{\rm HVAC} = \mu_{\rm HVAC} P_{\rm HVAC}$, where $P_{\rm HVAC}$ is the actual power consumed by HVAC systems and the main optimization variable/setpoint for each building, and $\mu_{\rm HVAC}$ is a constant indicating the performance of an HVAC system. The objective is to minimize a cost function of $P_{\rm HVAC}$ while maintaining occupants' comfort.

Since we aim to understand the impact of buildings' contribution to frequency regulation and overall energy consumption costs, we present the dynamics of building clusters:

$$\dot{\mathbf{x}}_b = \mathbf{A}_b \mathbf{x}_b + \mathbf{B}_{u_b} \mathbf{u}_b + \mathbf{B}_{w_b} \mathbf{w}_b \,, \tag{1}$$

where n_b is the total number of buildings in the network; $\mathbf{x}_b = [T_{\text{wall}} \ T_{\text{zone}}]^{\top} \in \mathbb{R}^{2n_b}, \mathbf{u}_b = [P_{\text{HVAC}}] \in \mathbb{R}^{n_b},$ and $\mathbf{w}_b = [T_{\text{amb}} \ \dot{Q}_{\text{sol}} \ \dot{Q}_{\text{int}}]^{\top} \in \mathbb{R}^{3n_b}$ are vectors collecting the state, controllable input, and random uncontrollable input for all n_b buildings. In the absence of communication between buildings, the state-space matrices $\mathbf{A}_b, \mathbf{B}_{u_b}$, and \mathbf{B}_{w_b} are all block-diagonal.

III. OCCUPANCY-BASED BUILDING CONSTRAINTS

An occupancy-based building MPC is further developed to simulate the impacts of occupancy on building demands and enable deeper energy savings. The ground truth occupancy information is first simulated based on a simulator from Lawrence Berkeley National Laboratory (LBNL) [32]. The LBNL's simulator generates the number of occupants at the whole building level based on large scale survey data. Then, an innovative prediction method, previously developed by authors [33] and specifically designed for building MPC is used to transfer the occupancy number to binary presence states and do "real" predictions based on the LBNL's "ground truth" simulation results for each rolling MPC. The occupancy predictions will forecast the lunch break as absence during certain time periods if the aggregated training data show a majority of the people leave the offices for lunch. Hence, the upper bounds of the building states x_b will increase during the lunch breaks. We introduce an occupancy-based slack relaxation that will be added on the upper bounds of the building states as follows

$$\mathcal{E}(\mathbf{O}_t) = \begin{cases} \alpha, & \text{if } \Gamma(\mathbf{O}_t) = \mathbf{0} \\ \max(\alpha, \mathbf{x}_b^{t-1} - \mathbf{x}_b^{\max}) & \text{if } \Gamma(\mathbf{O}_t) > \mathbf{1} \\ \mathbf{0}, & \text{if } \mathbf{0} < \Gamma(\mathbf{O}_t) \le \mathbf{1} \end{cases}$$
(2)

where $\mathcal{E}(\mathbf{O}_t)$ is an occupancy-based slack relaxation function based on binary occupancy predictions, \mathbf{x}_b^{\max} is the upper bound of the building states, and $\mathbf{O}_t = \mathbf{s}_t$ is the predicted binary occupancy state at optimized time step t in a rolling building MPC. The factor α is a predefined constraint adjustment threshold for building states. In other words, α describes how much the building zone temperature will increase when people are absent. However, function Γ is defined to avoid impractical settings of the factor α that will cause infeasible solutions of the building MPCs. This function is used to avoid infeasible solutions for BtG integrations and defined as follows

$$\Gamma(\mathbf{O}_t) = \mathbf{O}_t + \max(\mathbf{0}, \mathbf{x}_h^{t-1} - \mathbf{x}_h^{\max})$$
 (3)

where \mathbf{x}_b^{t-1} is the previous building state, and $\mathbf{x}_b^{\text{max}}$ is the upper bound of building states constraints. This empirically derived relaxation of (2) and (3) is designed to balance the feasibility of the MPC solver and the savings from the MPC. Note that the infeasible solutions are usually caused by the uncertain change of building states constraints based on the occupancy predictions. Owing to the upper limit on the cooling power and the building disturbances (i.e., large solar heat gains or internal heat gains at certain periods), building states or cooling power may not be able to satisfy constraints simultaneously for both cooling power and zone states. We will use the occupancy-based model as constraints to the overall BtG problem.

IV. BUILDING-INTEGRATED POWER NETWORK: DYNAMICS CONNECTION TO OPF

In this section, we present the dynamics of buildingintegrated power network and define the main variables involved in the BtG integration framework. In addition, we discuss the connection of BtG integration model with the optimal power flow (OPF).

A. DAE Dynamics of a Power Network with Building Loads

Let $\mathcal{B}=\{1,\ldots,n\}$ and $\mathcal{G}=\{1,\ldots,n_g\}$ denote the sets of buses and generators in a power network. Also, let \mathcal{N}_k be the neighborhood set of adjacent nodes connected to the k^{th} bus. Generators are indexed by $m\in\mathcal{G}$. The mechanical input power to the m^{th} generator is denoted by P_m . Define generator-to-node and building-to-node incidence matrices $\mathbf{\Gamma}\in\mathbb{R}^{n\times n_g}$ and $\mathbf{\Pi}\in\mathbb{R}^{n\times n_b}$ with entries given by:

$$\gamma_{k,m} = \begin{cases} 1 & \text{if the } m^{\text{th}} \text{ generator is connected to bus } k \\ 0 & \text{otherwise,} \end{cases}$$

$$\pi_{k,l} = \left\{ \begin{array}{cc} 1 & \quad \text{if the k^{th} bus is connected to building l} \\ 0 & \quad \text{otherwise.} \end{array} \right.$$

The transients of the k^{th} bus in a power network can be modeled by the swing equation which relates the rotor angle δ with the angular velocity $\dot{\delta}$ and angular acceleration $\ddot{\delta}$ [34]. Define M_k and D_k as the inertia and damping coefficients of the generator located k^{th} bus; if the k^{th} bus does not have a generator, then $M_k = D_k = 0$. The swing equation for the k^{th} bus $(\forall k \in \mathcal{B})$ can be written as:

$$M_k \ddot{\delta}_k + D_k \dot{\delta}_k = \gamma_{k,m} P_m - P_{L_k} - \sum_{j \in \mathcal{N}_k} b_{kj} \sin(\delta_k - \delta_j). \tag{4}$$

The load at bus k, P_{L_k} , can be written as follows: $P_{L_k} = D_k' \dot{\delta}_k + P_{\mathrm{BL}_k} + \sum_{l=1}^{n_b} \pi_{k,l} P_{\mathrm{bldg}}^{(l)}$, where $D_k' \dot{\delta}_k$ denotes the frequency-sensitive uncontrollable load at bus k; P_{BL_k} denotes the frequency-insensitive uncontrollable base-loads; $\sum_l \pi_{k,l} P_{\mathrm{bldg}}^{(l)}$ defines the load from buildings indexed by l and attached to bus k that are participating in regulation, defined as $P_{\mathrm{bldg}}^{(l)} = P_{\mathrm{HVAC}}^{(l)} + P_{\mathrm{misc}}^{(l)}$, where $l \in \{1, 2, \ldots, n_b\}$ is index of buildings. $P_{\mathrm{HVAC}}^{(l)}$ denotes the portion of controllable power consumption of building l, while $P_{\mathrm{misc}}^{(l)}$ represents the uncontrollable miscellaneous power consumption of building l. We can now rewrite (4) as:

$$M_k \ddot{\delta}_k + D_k \dot{\delta}_k = -\sum_{j \in \mathcal{N}_k} b_{kj} \sin(\delta_k - \delta_j)$$

$$+ \gamma_{k,m} P_m - D_k' \dot{\delta}_k - P_{\text{BL}_k}$$

$$- \sum_{l=1}^{n_b} \pi_{k,l} \left(P_{\text{HVAC}}^{(l)} + P_{\text{misc}}^{(l)} \right).$$
 (5)

In (5), P_m for generator bus m can be written as $P_m = \bar{P}_m + \Delta P_m$, where \bar{P}_m is a solution of an optimal power flow problem—computed every 15 minutes—and ΔP_m is the deviation from the setpoint \bar{P}_m , which will be furnished by the proposed BtG integration framework.

Let $\hat{\delta}_k = \omega_k$, where $\omega_k = \omega_k^{\text{true}} - \omega_0$, where ω_k^{true} is the actual frequency of the kth bus (ω_0 is the synchronous frequency). The resulting state-space model is a nonlinear descriptor system (or a DAE), and can be written as:

$$\mathbf{E}_{g}\dot{\mathbf{x}}_{g} = \mathbf{A}_{g}\mathbf{x}_{g} + \mathbf{\Phi}(\boldsymbol{\delta}) + \mathbf{A}_{u_{b}}\mathbf{u}_{b} + \mathbf{B}_{u_{q}}\mathbf{u}_{g} + \mathbf{B}_{w_{q}}\mathbf{w}_{g}, \quad (6)$$

where $\mathbf{x}_g = [\delta_1 \dots \delta_n \ \omega_1 \dots \omega_n]^\top = [\boldsymbol{\delta}^\top \ \boldsymbol{\omega}^\top]^\top$ is the state of the grid; $\boldsymbol{\Phi}(\boldsymbol{\delta})$ is the vectorized nonlinear power flow equations in (5); $\mathbf{u}_b = [P_{\text{HVAC}}^{(1)} \dots P_{\text{HVAC}}^{(n_b)}]^\top$ is the control input vector of the buildings, as defined in (1), and $\mathbf{u}_g = \bar{\mathbf{u}}_g + \Delta \mathbf{u}_g = [\bar{P}_1 + \Delta P_1 \dots \bar{P}_{n_g} + \Delta P_{n_g}]^\top$ is the power network's control variable; $\mathbf{w}_g = [\mathbf{w}_{\text{BL}}^\top, \mathbf{w}_{\text{misc}}^\top]^\top = [P_{\text{BL}_1} \dots P_{\text{BL}_n}, P_{\text{misc}}^{(1)} \dots P_{\text{misc}}^{(n_b)}]^\top$ is a random vector collecting the nodal base loads and miscellaneous building loads. Load forecasting is a very mature area; in the sequel, the forecast of \mathbf{w}_g , denoted by $\hat{\mathbf{w}}_g$, is assumed to be available.

B. Connection to the Optimal Power Flow

Recall that $\mathbf{u}_g = \bar{\mathbf{u}}_g + \Delta \mathbf{u}_g$, where $\bar{\mathbf{u}}_g$ is the vector containing the setpoints for the generators, and $\Delta \mathbf{u}_g$ is the real-time deviation from these setpoints that automatically drives the power grid to stability after load deviations or disturbances. Typically, the setpoints are computed every 5–15 minutes through solving economic dispatch or OPF routines [34]. A linearized OPF (LOPF) problem can be written as:

$$\textbf{LOPF:} \quad \underset{\bar{\mathbf{u}}_g = \{\bar{u}_{g_i}\}_{i=1}^{n_g}}{\operatorname{minimize}} \ J(\bar{\mathbf{u}}_g) = \bar{\mathbf{u}}_g^{\top} \mathbf{J}_{u_g} \bar{\mathbf{u}}_g + \mathbf{b}_{u_g}^{\top} \bar{\mathbf{u}}_g + c_{u_g} \text{(7a)}$$

subject to
$$\bar{\mathbf{u}}_q^{\min} \le \bar{\mathbf{u}}_g \le \bar{\mathbf{u}}_q^{\max}$$
 (7b)

$$(\mathbf{\Gamma}\bar{\mathbf{u}}_{q} - \mathbf{\Pi}(\mathbf{u}_{b} + \hat{\mathbf{w}}_{misc}) - \hat{\mathbf{w}}_{BL})^{\top} \mathbf{1}_{n} = 0$$
 (7c)

$$|\mathbf{L}_{\mathrm{ptdf}} \left(\mathbf{\Gamma} \bar{\mathbf{u}}_{q} - \mathbf{\Pi} (\mathbf{u}_{\mathrm{b}} + \hat{\mathbf{w}}_{\mathrm{misc}}) - \hat{\mathbf{w}}_{\mathrm{BL}} \right) | \leq \mathbf{F}^{\mathrm{max}} , \quad (7d)$$

where $J(\bar{\mathbf{u}}_g)$ is a convex cost function that represents the generators' cost curves; \mathbf{u}_b and $\hat{\mathbf{w}}_{\mathrm{misc}}$ are vectors of building HVAC and (forecasted) miscellaneous loads; $\hat{\mathbf{w}}_{\mathrm{BL}}$ is the vector of (forecasted) base loads; vector $\Gamma \bar{\mathbf{u}}_g - \Pi(\mathbf{u}_b + \hat{\mathbf{w}}_{\mathrm{misc}}) - \hat{\mathbf{w}}_{\mathrm{BL}}$ represents the nodal power injections; $\mathbf{1}_n \in \mathbb{R}^n$ is a vector of all ones; $\mathbf{F}^{\mathrm{max}} \in \mathbb{R}^{n_l}$ is the vector containing the thermal limits for real power flow on the n_l branches of the network; and $\mathbf{L}_{\mathrm{ptdf}} \in \mathbb{R}^{n_l \times n}$ is a matrix of power transfer distribution factors [35]. The constraints represent the safety upper and lower bounds on the generator's active power while ensuring the supply-demand balance and the satisfaction of line flow limits. This formulation is useful in the next sections.

V. How Can Buildings Impact Power Grids?

In the previous section, we formulate the dynamics of the buildings-integrated power network. In (6), the presence of \mathbf{u}_b exemplifies the control potential that buildings have on power system operation and control, and hence the BtG integration. Here, we investigate the discrepancies in time-scales between the building (1) and power network dynamics (6) and discuss a formulation of the joint optimal control problem that addresses the time-scale discrepancies.

A. Addressing the Time-Scales Discrepancy

The formulated dynamics in Sections II and IV clearly operate in two different time-scales. While grid regulation problems and mechanical input power variations are often in seconds, the building dynamics and controls are much slower. For example, temperatures in buildings change slowly in

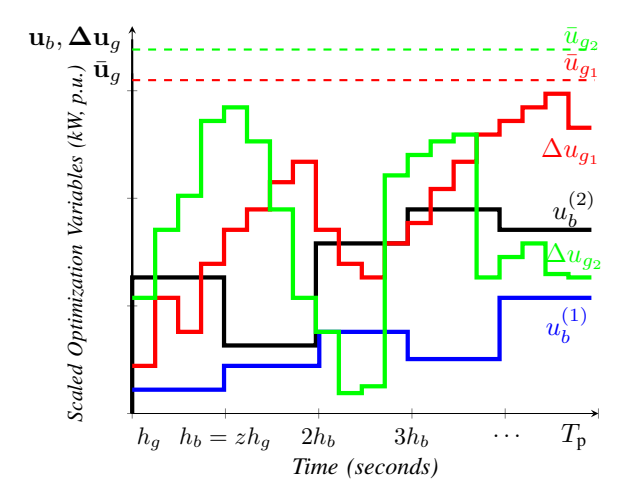


Fig. 1. The figure illustrates hypothetical solutions to a joint optimal control problem with multiple time-scales for a buildings-integrated power network. The quantities h_b, h_g, T_p are the building and grid sampling periods and the prediction horizon. Note that $h_b >> h_g$ and $h_b/h_g = z$, where $z \in \mathbb{N}_+$.

comparison with frequencies and voltages in power networks.

To overcome this limitation, we assume the following. Local optimal control laws for buildings are computed at different time-steps than local optimal control laws for generators. This approach reflects the physical realities for these systems, and this consideration can be imposed via constraints in the optimal control problem, whose construction is the objective of this section. Since buildings possess slower dynamic behavior, we restrict the controls of buildings to be fixed for the faster time-scale of the power network. Fig. 1 illustrates this idea. Consider a hypothetical network with two generators and two commercial buildings, making up a total of six control variables $(\mathbf{u}_b, \bar{\mathbf{u}}_a, \Delta \mathbf{u}_a)$. The optimal deviations from the generators' controls fluctuate at a higher rate than the building controls, whereas the set-points for generators change once for a single prediction horizon as shown in Fig. 1. Given this integration scheme, and since hard constraints are to be imposed on the grid and building dynamics, model predictive control (MPC) becomes the only viable solution to solve the joint optimal control problem.

B. Discretization of DAEs via Gear's Method

Another challenge facing BtG integration is the presence of algebraic equations in (6) emerging from power flows of load nodes. Here, we present a simple, yet high-fidelity discretization routine for two dynamical systems with different time-scales and dynamic algebraic constraints. The routine is based on Gear's method [36]. Note that for the discretization purposes, we use the linearized power flows by assuming that $\sin(\delta_i - \delta_j) = \delta_i - \delta_j$.

First, we assume that the sampling times for the power grid [cf. (6)] and building [cf. (1)] dynamics are respectively h_q and h_b ; note that $h_b >> h_q$. The discretized dynamics of

the building-integrated power network can be written as

$$\mathbf{x}_{g}(k_{g}h_{g}) = \mathbf{f}_{g}(\mathbf{x}_{g}, \mathbf{u}_{g}, \mathbf{u}_{b}, \mathbf{w}_{g})$$

$$= \bar{\mathbf{A}}_{g} \sum_{i=1}^{s} \alpha_{i} \mathbf{E}_{g} \mathbf{x}_{g} (h_{g}(k_{g} - i))$$

$$+ \mathbf{B}_{0} \left(\mathbf{A}_{\mathbf{u}_{b}} \mathbf{u}_{b}(k_{g}h_{g}) + \mathbf{B}_{u_{g}} \mathbf{u}_{g}(k_{g}h_{g}) \right)$$

$$+ \mathbf{B}_{0} \mathbf{B}_{w_{g}} \mathbf{w}_{g}(k_{g}h_{g})$$
(8)

where $\bar{\mathbf{A}}_g = (\mathbf{E}_g - h_g \beta_0 \mathbf{A}_g)^{-1}, \mathbf{B}_0 = h_g \beta_0 \bar{\mathbf{A}}_g, \beta_0 = (\sum_{i=1}^s 1/i)^{-1}, \alpha_i = (-1)^{i+1} \beta_0 \sum_{j=i}^s j^{-1} \binom{j}{i}$; k_g is the time-step for the grid dynamics. This method requires a set of s initial conditions. Similarly, the discrete form of (1) can be written as follows:

$$\mathbf{x}_b(k_b h_b) = \mathbf{f}_b(\mathbf{x}_b, \mathbf{u}_b, \mathbf{w}_b) = \bar{\mathbf{A}}_b \sum_{i=1}^s \alpha_i \mathbf{x}_b (h_b(k_b - i)) + \mathbf{B}_1 \left(\mathbf{B}_{u_b} \mathbf{u}_b(k_b h_b) + \mathbf{B}_{w_b} \mathbf{w}_b(k_b h_b) \right), \quad (9)$$

where k_b is time-step for buildings' dynamic operation. Gear's discretization amounts to a backward Euler-like implicit method. The principal merit of implicit methods is that they are typically more stable for solving systems with a larger step size h, while still performing well for systems with faster time-constants [36]. A simple simulation indeed shows that Gear's method returns accurate state-solution for the building and grid dynamics.

C. OBtG: Occupancy-based Buildings-to-Grid Optimization

The joint optimal control problem, Occupancy-based Buildings-to-Grid (OBtG), is formulated in (11). The variables, cost function, and constraints of OBtG are as follows. T_p is the prediction horizon and the formulation above only shows the MPC for one prediction horizon; t is the initial starting point of the MPC (note that power grid-MPC has been used before [37], [38]). $\mathbf{U}_b = \{\mathbf{u}_b(t+h_b), \mathbf{u}_b(t+2h_b), \ldots, \mathbf{u}_b(t+T_p)\}, \Delta \mathbf{U}_g = \{\Delta \mathbf{u}_g(t+h_g), \Delta \mathbf{u}_g(t+2h_g), \ldots, \Delta \mathbf{u}_g(t+T_p)\},$ and $\bar{\mathbf{u}}_g$ are the three sets of optimization variables that we defined previously.

Also, the cost function is defined as in (10) (in the next page) which adds the LOPF costs to the average of the building and grid control costs: $J(\bar{\mathbf{u}}_g)$ is the LOPF cost function (7a) and $\mathbf{c}_b(t+k_bh_b)$ is a time-varying vector representing the cost of electricity at time $t+k_bh_b$. $\mathbf{Q} \in \mathbb{R}^{2n\times 2n}$ and $\mathbf{R} \in \mathbb{R}^{n_g \times n_g}$ are positive semi-definite penalty matrices for the grid dynamics, with penalization to the deviations in the frequencies of the generators and the magnitude of the control actions—see [34] for a similar regulation penalties.

Constraints (11b)–(11d) depict the dynamics of the building-integrated power grid, as well as lower and upper bounds on the states and inputs of the grid states and controls. Constraints (11e)–(11g) represent the building cluster dynamics and the bounds on the states and inputs of the individual buildings where $\mathcal{E}(\mathbf{O}_t)$ is the occupancy-based slack relaxation function defined early in (2). Constraint (11h) imposes the constraints of the LOPF as discussed in the previous section. The final constraint (11i) represents the idea of the time-scales integration, as illustrated in Fig. 1, whereby the

$$f(\Delta \mathbf{U}_g, \bar{\mathbf{u}}_g, \mathbf{U}_b) = J(\bar{\mathbf{u}}_g) + \frac{h_b}{T_p} \sum_{k_b=1}^{T_p/h_b} \left[\mathbf{c}_b^{\top}(t + k_b h_b) \mathbf{u}_b(t + k_b h_b) \right] + \frac{h_g}{T_p} \sum_{k_a=1}^{T_p/h_g} \left[\Delta \mathbf{u}_g^{\top}(t + k_g h_g) \mathbf{R} \Delta \mathbf{u}_g(t + k_g h_g) \right]$$
(10)

building control variables (8) are kept constant between two consecutive building instances. Since $h_b > h_g$, we assume that between two consecutive building sampling instances (i.e., k_bh_b and $(k_b+1)h_b$), the building controls $u_b(k_bh_b)$ are all constant variables to be found. Hence, for all $\forall k_gh_g \in [k_bh_b, (k_b+1)h_b)$, $\mathbf{u}_b(k_bh_b) = \mathbf{u}_b(k_gh_g) = \bar{\mathbf{u}}_b$.

OBtG:

$$\min_{\mathbf{U}_{b}, \Delta \mathbf{U}_{g}, \bar{\mathbf{u}}_{g}} f(\Delta \mathbf{U}_{g}, \bar{\mathbf{u}}_{g}, \mathbf{U}_{b}) \qquad (11a)$$
s.t. $\mathbf{x}_{g}(t + k_{g}h_{g}) = \mathbf{f}_{g}(\mathbf{x}_{g}, \mathbf{u}_{g}, \mathbf{u}_{b}, \hat{\mathbf{w}}_{g} \mid t, s) \qquad (11b)$

$$\Delta \mathbf{u}_{g}^{\min} \leq \Delta \mathbf{u}_{g}(t + k_{g}h_{g}) \leq \Delta \mathbf{u}_{g}^{\max} \qquad (11c)$$

$$\mathbf{x}_{g}^{\min} \leq \mathbf{x}_{g}(t + k_{g}h_{g}) \leq \mathbf{x}_{g}^{\max} \qquad (11d)$$

$$\forall k_{g} \in \{1, \dots, T_{p}/h_{g}\}$$

$$\mathbf{x}_{b}(t + k_{b}h_{b}) = \mathbf{f}_{b}(\mathbf{x}_{b}, \mathbf{u}_{b}, \hat{\mathbf{w}}_{b} \mid t, s) \qquad (11e)$$

$$\mathbf{u}_{b}^{\min} \leq \mathbf{u}_{b}(t + k_{b}h_{b}) \leq \mathbf{u}_{b}^{\max} \qquad (11f)$$

$$\mathbf{x}_{b}^{\min} \leq \mathbf{x}_{b}(t + k_{b}h_{b}) \leq \mathbf{x}_{b}^{\max} + \mathcal{E}(\mathbf{O}_{t}) \qquad (11g)$$

$$\forall k_{b} \in \{1, \dots, T_{p}/h_{b}\}$$

$$(7b), (7d) \qquad (11h)$$

$$\mathbf{u}_{b}(t + k_{g}h_{g}) = \bar{\mathbf{u}}_{b} = \mathbf{u}_{b}(t + k_{b}h_{b}) \qquad (11i)$$

$$\forall k_{g}h_{g} \in [k_{b}h_{b}, (k_{b} + 1)h_{b}).$$

Algorithm 1 Online OBtG and LOPF Integration

```
1: input: OBtG forecasts and parameters
 2: output: \{\bar{\mathbf{u}}_g^*, \Delta \mathbf{u}_g^*, \mathbf{u}_b^*\}
 3: while t < T_{\text{final}}
               if t = \kappa T_p (multiple of T_p)
 4:
                   solve OBtG (11) for \mathbf{U}_b^*, \Delta \mathbf{U}_g^*, \bar{\mathbf{u}}_g^*
 5:
                   apply \bar{\mathbf{u}}_{q}^{*} \ \forall t \in [\kappa T_{p}, (\kappa+1)T_{p}]
 6:
                   apply \mathbf{U}_b^*(1) \ \forall t \in [t, t + h_b]
 7:
                   apply \Delta \mathbf{U}_{q}^{*}(1) \ \forall t \in [t, t + h_{q}]
 8:
                   discard \mathbf{U}_{b}^{*}(2:\mathrm{end}), \Delta\mathbf{U}_{a}^{*}(2:\mathrm{end})
 9.
               else if (t = \kappa_1 h_g) \wedge (t \neq \kappa_2 T_p) \wedge (t \neq \kappa_3 h_b)
10:
                   solve (11) without \bar{\mathbf{u}}_g, \mathbf{U}_b, while eliminating (11e)–(11i)
11:
12:
                   apply \Delta \mathbf{U}_{q}^{*}(1) \ \forall t \in [t, t + h_{q}]
                   discard \Delta \mathbf{U}_{q}^{*}(2:end)
13:
               else if (t = \kappa_1 \check{h}_b) \wedge (t \neq \kappa_2 T_p)
14:
                   solve (11) without \bar{\mathbf{u}}_g, (11h), and J(\bar{\mathbf{u}}_g)
15:
16:
                   apply \mathbf{U}_b^*(1) \ \forall t \in [t, t + h_b]
                   apply \Delta \mathbf{U}_q^*(1) \ \forall t \in [t, t + h_g]
17:
                   discard \mathbf{U}_b^*(2:\mathrm{end}), \Delta \mathbf{U}_q^*(2:\mathrm{end})
18:
19:
              end if
              t \leftarrow t + h_q
20:
21: end while
```

Algorithm 1 illustrates a routine that implements OBtG's rolling horizon window along with the integration of the LOPF problem. The proposed algorithm solution mimics the idea depicted in Fig. 1. Given the OBtG parameters (including the first s-initial steps of the discretized dynamics), the algorithm computes the optimal solutions to the LOPF

problem and the joint MPC.

We assume that $h_g < h_b < T_p << T_{\text{final}}$ and h_b/h_g , T_p/h_b , T_p/h_q are all positive integers. The algorithm starts by finding the solution to the generator's operating points $\bar{\bf u}_a$ for any multiple of the prediction horizon T_p , as well as the deviation from this set-point $\Delta \mathbf{u}_q$ and \mathbf{u}_b up until the next planning horizon, and so on. As in classical MPC routines, only the first instance of the optimal control trajectory is applied, while the rest are discarded. Note that the OBtG with LOPF is only solved for when t (the counter) is a multiple of T_p . If t is not a multiple of T_p , but a multiple of the building's sampling time h_b , the building and grid controls are computed. The final case captures the gap between the two time-scales: where the building and grid controls are applied, the building controls are kept constant from the previous optimal computations, while grid controls are computed in the meantime for every grid sampling time.

VI. CASE STUDIES

A. Experimental Setup

For the building HVAC system, one day of summer weather data collected by a local weather station is used. The overall coefficient of performance of the HVAC systems in buildings is assumed to be constant and equal to 3. The maximum cooling power is limited to 330KW per building. Office hours are defined from 7:30am to 8:00pm, while early start-up of the system is set from 7:00 am to 7:30 am.

The set-point for office hours is $21.4 \pm 0.6^{\circ}\text{C}$ while the set-point for non-office hours is $23.5 \pm 0.5^{\circ}\text{C}$. A night setback strategy for non-office hours is used for the HVAC baseline simulation. All the commercial building occupancy profiles are simulated and generated using the LBNL occupancy simulator [32] to produce the synthetic ground truth occupancy data for individual building. We first introduce the occupancy density multiplier based on the randomized building size. Then, the original algorithm is modified to randomize the user-predefined parameters of the occupancy transitions among zones, including private cubicles, meeting spaces, auxiliary rooms the first arrival and the last departure times. The example occupancy profile is presented using 300 randomized buildings in Figure 2. The data used for the simulations are available upon request.

B. Results and Comparison

This study investigates two cases: 1) a decoupled baseline, and 2) a centralized OBtG integration with occupancy predictions. For the decoupled baseline case, we use the traditional bang-bang approach for building simulations and perform a separate grid MPC where the building load is merely input to the grid operations. The building controls are assumed to use bang-bang control of ideal cooling demands. This means that

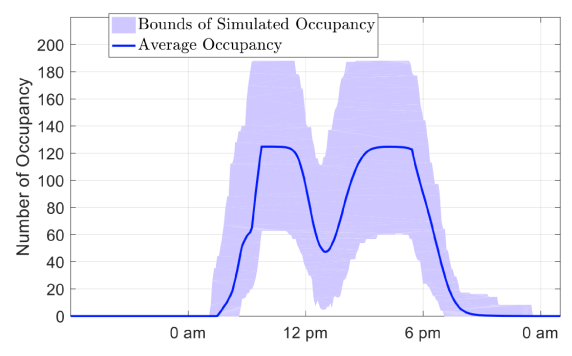


Fig. 2. Simulated "ground truth" form the LBNL simulator [32].

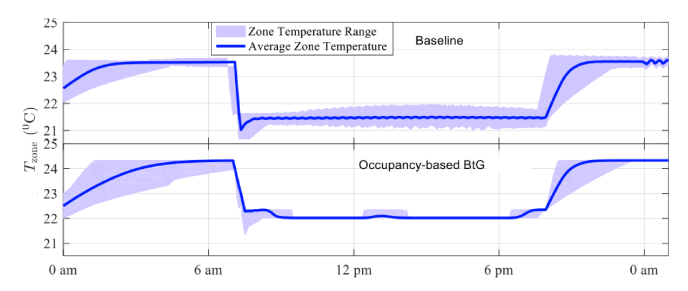
the HVAC system only has two modes: "off" for no cooling, and "on" for ideal cooling to meet with loads. However, the cooling amount may vary based on an ideal cooling calculation [39]. The second case is the complete occupancy-based OBtG (11) and Algorithm 1. Simulation results for one day based on case9 from [35] are presented in Fig. 3. Extended simulations are performed on the IEEE case14

TABLE I Cost comparison for the two scenarios (the costs are in \$1.000).

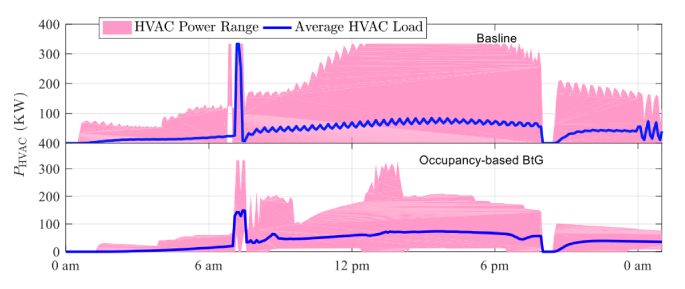
Test	Cost Type	Baseline	OB BtG MPC
Case			
	Frequency	1137.56	1.34 (99%)
Case	Penalty		
9	Generator	227.03	223.27 (1.5%)
	Generation		
	Building	422.75	381.98 (9.6%)
	Energy Cost		
	Total Cost	1787.34	606.59 (66%)
	Frequency	950.52	1.61 (99%)
Case	Penalty		
14	Generator	367.26	363.78 (0.5%)
	Generation		
	Building	464.08	420.14 (9.4%)
	Energy Cost		
	Total Cost	1781.92	785.55 (56%)

grid system with similar testing configurations above. This section provides the detailed cost analysis and comparison based on case9 and case14 for all tested two cases. Table I shows all the costs for the two scenarios during the one week test simulation with absolute amounts and saving percentages respectively (the figures only show one day).

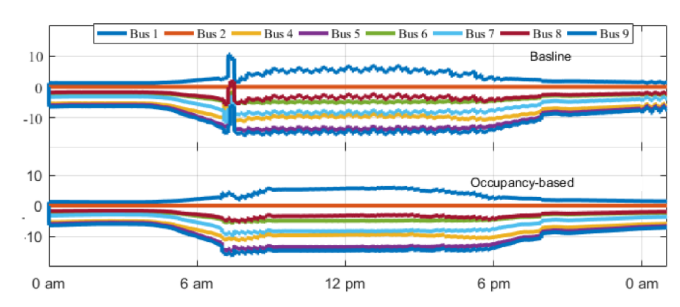
Comparing frequency penalties for the two scenarios of all grid cases, there are significant decreases of the frequency costs during the grid operations when the OBtG is used. The grid frequencies experience large deviations from its nominal value (60 Hz) for the baseline simulations. However, the frequency deviations for OBtG are much smaller. Similar conclusions can be made for case14 simulation. In contrast, the costs of electricity generation are very close to each other for all test scenarios. Maximum 1.5% of cost saving can be observed for both case9 and case14 systems although the maximum absolute saving amount is around \$4,000. Meanwhile, the building costs based on the real-time prices show larger savings for the OBtG case comparing to the baseline scenario. The maximum saving is around 9.6% for the



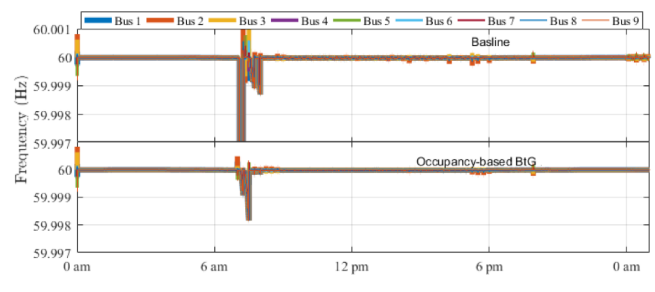
(a) Building zone state (temperature) responses.



(b) Optimized bulidng control inputs (HVAC cooling power).



(c) Bus angle responses for all buses with angle of bus 3 as the reference.



(d) Grid frequency responses for all buses.

Fig. 3. Comparison of the performance of the baseline optimization framework (top subfigures) and the OBtG (bottom) in terms of the building and grid's states.

occupancy-based BtG case for that specific day simulation. By calculating the total costs, OBtG produces a total of 66% of savings for case9 and 56% for case14. The majority of the savings are due to the frequency regulation and building energy savings.

VII. PAPER SUMMARY AND FUTURE WORK

We introduce a computational framework to integrate the local decisions of building operators, namely the HVAC system energy consumption, with that of generators in smart grids. The framework is cognizant of the occupancy behavior of people inside buildings. We also explore the impact of such

a BtG framework on frequency regulation. The presented case studies illustrate that an occupancy-aware BtG framework has the potential to provide frequency regulation, while reducing energy consumption. Although only the generator and HVAC control variables are modeled in this paper, the presented framework can be easily extended to incorporate distributed energy resources and optimal power flow formulations in distribution networks, with electric vehicles and deferrable loads. We plan to study these important extensions to this work.

REFERENCES

- [1] T. M. Lawrence, M.-C. Boudreau, L. Helsen, G. Henze, J. Mohammadpour, D. Noonan, D. Patteeuw, S. Pless, and R. T. Watson, "Ten questions concerning integrating smart buildings into the smart grid," *Building and Environment*, vol. 108, no. Supplement C, pp. 273 – 283, 2016. [Online]. Available: http://www.sciencedirect.com/science/article/pii/S0360132316303171
- [2] J. Qi, Y.-J. Kim, C. Chen, X. Lu, and J. Wang, "Demand response and smart buildings: A survey of control, communication, and cyberphysical security," ACM Transactions on Cyber-Physical Systems, vol. 1, no. 3, pp. 1–28, 2016.
- [3] G. Stamatescu, I. Stamatescu, N. Arghira, V. Calofir, and I. Fa-garasan, "Building cyber-physical energy systems," arXiv preprint arXiv:1605.06903, 2016.
- [4] M. Razmara, G. R. Bharati, M. Shahbakhti, S. Paudyal, and R. D. R. III, "Bilevel optimization framework for smart building-to-grid systems," *IEEE Transactions on Smart Grid*, vol. PP, no. 99, pp. 1–1, 2016
- [5] E. Bilgin, M. C. Caramanis, I. C. Paschalidis, and C. G. Cassandras, "Provision of regulation service by smart buildings," *IEEE Transactions on Smart Grid*, vol. 7, no. 3, pp. 1683–1693, May 2016.
- [6] P. Zhao, G. P. Henze, S. Plamp, and V. J. Cushing, "Evaluation of commercial building hvac systems as frequency regulation providers," *Energy and Buildings*, vol. 67, pp. 225–235, 2013.
- [7] P. Zhao, G. Henze, and M. Brandemuehl, "Dynamic frequency regulation resources of commercial buildings through combined building system resources using a supervisory control methodology," *Energy and Buildings*, vol. 86, pp. 137–150, 2015.
- [8] D. Blum and L. M. Norford, "Dynamic simulation of regulation demand response by hvac systems," in 2014 ASHRAE/IBPSA Building Simulation Conference, Atlanta, GA, 2014.
- [9] H. Hao, Y. Lin, A. S. Kowli, P. Barooah, and S. Meyn, "Ancillary service to the grid through control of fans in commercial building hvac systems," *IEEE Transactions on smart grid*, vol. 5, no. 4, pp. 2066–2074, 2014.
- [10] Y. Lin, P. Barooah, and J. L. Mathieu, "Ancillary services through demand scheduling and control of commercial buildings," *IEEE Trans*actions on Power Systems, vol. 32, no. 1, pp. 186–197, Jan 2017.
- [11] M. Mileti, A. Schirrer, and M. Kozek, "Load management in smart grids with utilization of load-shifting potential in building climate control," in *Smart Electric Distribution Systems and Technologies* (EDST), 2015 International Symposium on, Sept 2015, pp. 468–474.
- [12] A. Wagner, W. O'Brien, and B. Dong, Exploring Occupant Behavior in Buildings. Springer, 2018.
- [13] G. Y. Yun and K. Steemers, "Time-dependent occupant behaviour models of window control in summer," *Building and Environment*, vol. 43, no. 9, pp. 1471–1482, 2008.
- [14] W.-k. Chang and T. Hong, "Statistical analysis and modeling of occupancy patterns in open-plan offices using measured lighting-switch data," in *Building Simulation*, vol. 6, no. 1. Springer, 2013, pp. 23–32.
- [15] H. B. Gunay, W. O'Brien, I. Beausoleil-Morrison, and B. Huchuk, "On adaptive occupant-learning window blind and lighting controls," *Building Research & Information*, vol. 42, no. 6, pp. 739–756, 2014.
- [16] W. O'Brien and H. B. Gunay, "Mitigating office performance uncertainty of occupant use of window blinds and lighting using robust design," *Building Simulation*, vol. 8, no. 6, pp. 621–636, Dec 2015. [Online]. Available: https://doi.org/10.1007/s12273-015-0239-2
- [17] K. Ahmed, P. Pylsy, and J. Kurnitski, "Monthly domestic hot water profiles for energy calculation in finnish apartment buildings," *Energy and Buildings*, vol. 97, pp. 77–85, 2015.

- [18] B. Dong, B. Andrews, K. P. Lam, M. Höynck, R. Zhang, Y.-S. Chiou, and D. Benitez, "An information technology enabled sustainability test-bed (itest) for occupancy detection through an environmental sensing network," *Energy and Buildings*, vol. 42, no. 7, pp. 1038–1046, 2010.
- [19] B. Dong and K. P. Lam, "Building energy and comfort management through occupant behaviour pattern detection based on a large-scale environmental sensor network," *Journal of Building Performance Simulation*, vol. 4, no. 4, pp. 359–369, 2011.
- [20] —, "A real-time model predictive control for building heating and cooling systems based on the occupancy behavior pattern detection and local weather forecasting," in *Building Simulation*, vol. 7, no. 1. Springer, 2014, pp. 89–106.
- [21] A. Mirakhorli and B. Dong, "Occupant-behavior driven appliance scheduling for residential buildings," in *Building Simulation*. Springer, pp. 1–15.
- [22] M. Kummert, M.-A. Leduc, and A. Moreau, "Using mpc to reduce the peak demand associated with electric heating," in *Model predictive* control in buildings workshop, 2011.
- [23] A. Yahiaoui, J. Hensen, L. Soethout, and A. Paassen, "Model based optimal control for integrated building systems," in *Proceedings of the* 6th International Postgraduate Research Conference in the Built and Human Environment, at Delft, The Netherlands. Citeseer, 2006.
- [24] B. Dong, "Integrated building heating, cooling and ventilation control," Ph.D. dissertation, 2010.
- [25] M. Maasoumy, "Modeling and optimal control algorithm design for hvac systems in energy efficient buildings," 2014.
- [26] A. Afram and F. Janabi-Sharifi, "Theory and applications of hvac control systems a review of model predictive control (mpc)," *Building* and *Environment*, vol. 72, pp. 343 – 355, 2014.
- [27] J. R. Dobbs and B. M. Hencey, "Model predictive hvac control with online occupancy model," *Energy and Buildings*, vol. 82, pp. 675–684, 2014
- [28] L. Standardi, "Economic model predictive control for large-scale and distributed energy systems," 2015.
- [29] N. R. Patel, M. J. Risbeck, J. B. Rawlings, M. J. Wenzel, and R. D. Turney, "Distributed economic model predictive control for large-scale building temperature regulation," in *American Control Conference (ACC)*, 2016. IEEE, 2016, pp. 895–900.
- [30] C. Chen, J. Wang, Y. Heo, and S. Kishore, "Mpc-based appliance scheduling for residential building energy management controller," *IEEE Transactions on Smart Grid*, vol. 4, no. 3, pp. 1401–1410, Sept 2013.
- [31] A. F. Taha, N. Gatsis, B. Dong, A. Pipri, and Z. Li, "Buildings-to-grid integration framework," *IEEE Transactions on Smart Grid*, 2017, in press. [Online]. Available: https://arxiv.org/pdf/1706.05626.pdf
- [32] X. Feng, D. Yan, and T. Hong, "Simulation of occupancy in buildings," Energy and Buildings, vol. 87, pp. 348–359, 2015.
- [33] Z. Li and B. Dong, "A new modeling approach for short-term prediction of occupancy in residential buildings," *Building and Environment*, vol. 121, pp. 277–290, 2017.
- [34] J. Taylor, Convex Optimization of Power Systems. Cambridge University Press, 2015.
- [35] R. D. Zimmerman, C. E. Murillo-Sánchez, and R. J. Thomas, "Mat-power: Steady-state operations, planning, and analysis tools for power systems research and education," *Power Systems, IEEE Transactions on*, vol. 26, no. 1, pp. 12–19, 2011.
- [36] R. Sincovec, A. Erisman, E. Yip, and M. Epton, "Analysis of descriptor systems using numerical algorithms," *IEEE Transactions on Automatic Control*, vol. 26, no. 1, pp. 139–147, Feb 1981.
- [37] M. R. Almassalkhi and I. A. Hiskens, "Model-predictive cascade mitigation in electric power systems with storage and renewables—part i: Theory and implementation," *IEEE Transactions on Power Systems*, vol. 30, no. 1, pp. 67–77, 2015.
- [38] M. R. Almassalkhi, "Optimization and model-predictive control for overload mitigation in resilient power systems," Ph.D. dissertation, University of Michigan, 2013.
- [39] Z. Li and P. Rolando Vega PhD, "A hybrid model for electrical load forecasting-a new approach integrating data-mining with physics-based models," ASHRAE Transactions, vol. 121, p. 1GGG, 2015.